



Real-time discrimination of photon pairs using machine learning at the LHC

Sean Benson¹, Adrián Casais Vidal², Xabier Cid Vidal², Albert Puig Navarro³

¹*Nikhef National Institute for Subatomic Physics, Amsterdam, The Netherlands*

²*Instituto Galego de Física de Altas Enerxías (IGFAE), Universidade de Santiago de Compostela, Santiago de Compostela, Spain*

³*Physik-Institut, Universität Zürich, Zürich, Switzerland*

Abstract

ALPs and other as-yet unobserved B decays to di-photon final states are a challenge to select in hadron collider environments due to the large backgrounds that come directly from the pp collision. We present the strategy implemented by the LHCb experiment in 2018 to efficiently select such photon pairs. The fast neural network topology, implemented in the LHCb real-time selection framework achieves high efficiency across a mass range of 4–20 GeV/ c^2 . We discuss implications and future prospects for the LHCb experiment.

Submitted to SciPost Physics

1 Introduction

The $\gamma\gamma$ final state is interesting for a variety of reasons. On one hand, the decay of a B_s^0 meson to two photons remains unobserved and is described by an annihilation topology. It is sensitive to contributions from physics beyond the Standard Model (SM) including a fourth generation [1], an extended Higgs sector [2] and SUSY [3]. Previous measurements by the Belle and BaBar collaborations have set limits of $\mathcal{B}(B_s^0 \rightarrow \gamma\gamma) < 3.1 \times 10^{-6}$ at 90 % confidence level (CL) [4] and $\mathcal{B}(B^0 \rightarrow \gamma\gamma) < 3.3 \times 10^{-7}$ at 90 % CL [5], which are significantly above the SM predictions of $\mathcal{B}(B_s^0 \rightarrow \gamma\gamma) \sim (2 - 37) \times 10^{-7}$ and $\mathcal{B}(B^0 \rightarrow \gamma\gamma) \sim (1 - 10) \times 10^{-8}$ [6].

Undiscovered particles known as Axion-Like Particles (ALPs) could also be accessed through this final state. ALPs are pseudo Nambu-Goldstone bosons, associated to spontaneously broken approximate symmetries, which appear in several models and can solve many of the SM problems [7]. Probing very small couplings of ALPs to the SM sets indirectly constraints to the New Physics (NP) scale. In the SM sector, ALPs couple to gluons (which allows their production at the LHC) or photons (which can be used for their discovery). The mass of ALPs can be arbitrarily below the NP scale. In particular, for ALPs with a mass in the range between 5 and 10 GeV/ c^2 , the LHCb experiment, described in Ref. [8], has unique sensitivity for their discovery provided they can be selected by its trigger algorithms [7]. For masses below 5 GeV/ c^2 , LHCb may have sensitivity through other decay channels, as described in [9].

The maximum rate at which events can be read out of the LHCb detector is imposed by the front-end electronics and corresponds to ~ 1 MHz. In order to determine which events are kept, hardware triggers based on field-programmable gate arrays are used with a fixed latency of 4 μ s. Information from the ECAL, HCAL, and muon stations is used in separate L0 triggers. All events selected by L0 are transferred to the High Level Trigger (HLT). The HLT is a software application, executed on an event filter farm, that is implemented in the same Gaudi framework [10] as the software used for the offline reconstruction. It consists of two levels: an initial selection of high energy and/or displaced single- or double-particle signatures (HLT1) and a second level (HLT2), in which full offline reconstruction is available, allowing for more complex searches to be performed [11].

The study of these purely neutral modes at LHCb is challenging, but the use of $\gamma \rightarrow e^+e^-$ conversions in the detector material, which happens for around 25 % of photons, provides additional information to reduce the background levels. With offline selections already in place since Run 1, this paper describes the trigger strategy adopted in Run 2, where a set of trigger selections were introduced to select the $\gamma\gamma$ signature for the case of zero, one, and two photon conversions, labelled as *0CV*, *1CV* and *2CV*, respectively. An additional label *LL* and *DD* is used to distinguish photon conversions reconstructed as:

- Long tracks (*LL*): when all possible tracking information from every tracking station is available, implying that the parent particle decayed within about 1 metre of the *pp* interaction point
- Downstream tracks (*DD*): using only information from tracking stations different to the vertex locator, implying that the parent particle decayed after this.

The work presented in this paper builds on the strategy first introduced in 2015 to select only the $B_{(s)}^0$ decay [12], in which a selection was put in place for *0CV*, *1CV* *LL*,

$1CV\ DD$, and $2CV$ (which includes both LL and DD combinations). The new approaches to select candidates in a wider mass range are described for the $0CV$, $1CV\ LL$, and $1CV\ DD$ topologies. The $2CV$ selection remains as is described in Ref. [12]. Section 2 describes the method by which our signal decays are simulated, Section 3 describes the HLT1 strategy. Section 4 describes the HLT2 strategy, performance, and corresponding implementation. The prospects for the current dataset collected by LHCb in addition to that expected to be collected by the upgraded LHCb detector (during Run 3 of the LHC and beyond) are discussed in Section 5.

2 Simulating the signal B_s^0 and ALP decays

In order to simulate $B_s^0 \rightarrow \gamma\gamma$ decays, pp collisions are generated using PYTHIA [13] with a specific LHCb configuration [14]. Decays of hadronic particles are described by EVTGEN [15], in which final-state radiation is generated using PHOTOS [16]. The interaction of the generated particles with the detector, and its response, are implemented using the GEANT4 toolkit [17] as described in Ref. [18]. This allows accurate simulation of the different topologies of the decay, as photons may interact with the detector itself and subsequently decay to electron-positron pairs.

For the ALP signal, samples are generated using Madgraph v2.6 [19], with parameters taken from the ALP model described in Ref. [20]. The hadronization is performed by PYTHIA, and the rest of the simulation steps are identical to simulating the $B_s^0 \rightarrow \gamma\gamma$ decay. Three ALP masses are simulated: $5\text{ GeV}/c^2$, $10\text{ GeV}/c^2$, and $15\text{ GeV}/c^2$.

After the detector response has been simulated, the trigger reconstruction and associated selection requirements are simulated using data taking conditions similar to those of the 2017 LHCb running period, with mean interactions per bunch crossing of 1.3 and center-of-mass-energy of 13 TeV.

Throughout this paper, efficiencies are evaluated with respect to a set of loose requirements inspired by those applied in the analysis of other radiative decays (*e.g.* those in Refs. [21–23]). In summary,

- photons reconstructed as calorimeter energy clusters are required to have an energy above 6 GeV and a transverse energy with respect of the beam direction above 3 GeV;
- photons reconstructed as electron pairs are required to have a transverse momentum in excess of 2 GeV, have a mass below $60\text{ MeV}/c^2$ and be displaced with respect to the pp collision;
- the sum of transverse momentum of the two photons must be in excess of 6.5, 5.5 and 5 GeV/ c for the $0CV$, $1CV$ and $2CV$ cases, respectively; and
- diphoton candidates are required to have a combined transverse momentum above 3 GeV/ c and, in the case of $2CV$, to form a good vertex.

3 HLT1 strategy

The first trigger software level is required to reduce the input rate by a factor 10 from the output of the hardware trigger level. In order to achieve this, a search is made primarily

Table 1: Selection applied in the Hlt1B2GammaGamma and Hlt1B2GammaGammaHighMass HLT1 trigger selection. Energies and masses given here are computed with 2×2 cell clusters.

Requirement	HLT1(B)	HLT1(ALP)
$E_T(\gamma)$ [GeV]	> 3.5	> 5
$E_T(\gamma_1) + E_T(\gamma_2)$ [GeV]	> 8	> 11
$M(\gamma_1\gamma_2)$ [GeV/ c^2]	[3.5, 6.0]	[6.0, 11.0]
$p_T(\gamma_1\gamma_2)$ [GeV/ c]	> 2	> 5

Table 2: Percentage efficiency relative to all candidates accepted by the L0 hardware trigger for the B_s^0 and ALP samples.

Efficiency (%)	HLT1(B)	HLT1(ALP)
$B_s^0 \rightarrow \gamma\gamma$	3.3 ± 0.2	-
ALP 5 GeV	6.2 ± 0.5	0.6 ± 0.2
ALP 10 GeV	5.3 ± 0.3	6.7 ± 0.4
ALP 15 GeV	3.8 ± 0.3	10.5 ± 0.5

for high transverse momentum tracks or tracks with a high impact parameter with respect to the primary vertex. A detailed description of the HLT1 selections for 2018 can be found in Ref. [12]: in the case of photon conversions with at least one electron reconstructed as a long track, a generic inclusive single-track, MVA-based trigger selection is used [11]; in all other cases, the HLT1 strategy relies on a custom reconstruction approach using information from the calorimeter collected in the hardware trigger stage. This latter reconstruction technique, imposed by the limited time available for decisions in HLT1, applies simple approximations to calculate the mass of the photon pair with a minimum E_T requirement in a negligible time using only their energies as calculated in L0.

Two selections with a different set of requirements are used: a first one, referred to as HLT1(B), focused on the selection of B decays, and a second one, not included in Ref. [12], with stricter E_T requirements and with a wider mass range, which extends the reach to ALP masses above the B mass window (HLT1(ALP)). Their requirements are given in Table 1; it is worth noting that the E_T requirements of the HLT1(ALP) are very close to the saturation of the LHCb ECAL when using L0 energy clusters,¹ and therefore the true mass reach is higher than the requirement given in the table. The efficiency of the two selections relative to all candidates passed by the L0 hardware trigger is given in Table 2.

4 HLT2 strategy

The second trigger software level performs a more complete event reconstruction. In HLT2, over 400 multibody decay signatures are searched for in parallel, with candidate

¹Calorimeter clusters in L0 are made up of 2×2 calorimeter cells. As a consequence, the mass that can be reconstructed at L0 level is limited by the saturation of these 4 cells of the cluster. This limitation will not be present in the final analysis, as the offline reconstruction allows to build larger clusters.

Table 3: Sample sizes for the signal decays and background after reconstruction and trigger requirements.

Sample	$1CV\ LL$	$1CV\ DD$	$0CV$
$B_s^0\gamma\gamma$	9940	17368	36844
ALPs	229	420	233
Background	228	393	457

selection information equivalent in quality to that used by analysts offline.

4.1 Training sample preparation

The first step in designing an HLT2 strategy is to collect representative samples of signal and background in order to train the neural network (NN) classifiers. For the case of the signal, *i.e.* B_s^0 and ALP decays, simulated data is used, which is generated as described in Sec. 2. In order to describe the background, proton-proton collisions collected by the LHCb collaboration during 2017 are used, in which the high level trigger selected candidates randomly.

Since the intention is to implement a NN inside the trigger software, no selection requirement was imposed that was less efficient than the initial requirements described in Sec. 2, in order to generate the largest possible NN training sample.

In the training of the NN, a random subset of the $B_s^0 \rightarrow \gamma\gamma$ sample is taken, such that efficiencies of the ALP signal and B_s^0 decay remain similar. The yields of the samples are provided in Table 3.

4.2 Multi-layer perceptron training and implementation

A multilayer perceptron (MLP) is chosen for the NN updates. A Scikit-learn implementation is chosen [24] due to the relative simplicity of the topology that allows for quick evaluation in real-time environments in association with the NNDrone package [25]. The model is created as

```

1 from sklearn.neural_network import MLPClassifier
2 classifier = MLPClassifier(activation='logistic'
3   , alpha=1e-05, batch_size='auto',
4   beta_1=0.9, beta_2=0.999, early_stopping=False,
5   epsilon=1e-08, hidden_layer_sizes=(3, 2),
6   learning_rate='constant', learning_rate_init=0.001,
7   max_iter=200, momentum=0.9,
8   nesterovs_momentum=True, power_t=0.5, random_state=1,
9   shuffle=True, solver='lbfgs', tol=0.0001,
10  validation_fraction=0.1, verbose=False, warm_start=False)

```

In order to train the MLP for each topology, different variables are found to have different separation powers. The following variables are used as a feature for one or more of the NN models:

- The transverse momentum of the parent B_s^0 or ALP candidate ($X p_T$).
- The impact parameter significance of the B_s^0 or ALP candidate with respect to the best primary vertex ($X IP \chi^2$), defined as the difference in χ^2 of a given PV reconstructed with and without the considered particle.
- The invariant mass of the electron-positron combination in a photon conversion.
- The probability that the photon candidate is not a π^0 meson based on a combination of calorimeter information (γ prob).
- Asymmetry of the p_T of the two photon candidates (p_T asym).
- The ratio of the candidate ECAL energy deposit between the 2×2 and 3×3 clusters (γ Calo E49).
- The output of a multi-variate classifier trained using various inputs corresponding to calorimeter shape variables (γ shower shape).

The signal and background distributions for each topology are given in Appendix A.

The samples are split into training and test data, where half of the data is used for training and the other half used for testing. The output distributions of the trained models for both the test and training samples are given in Fig. 1. Good agreement can be seen in all training and test comparisons, meaning the models show few signs of overtraining.

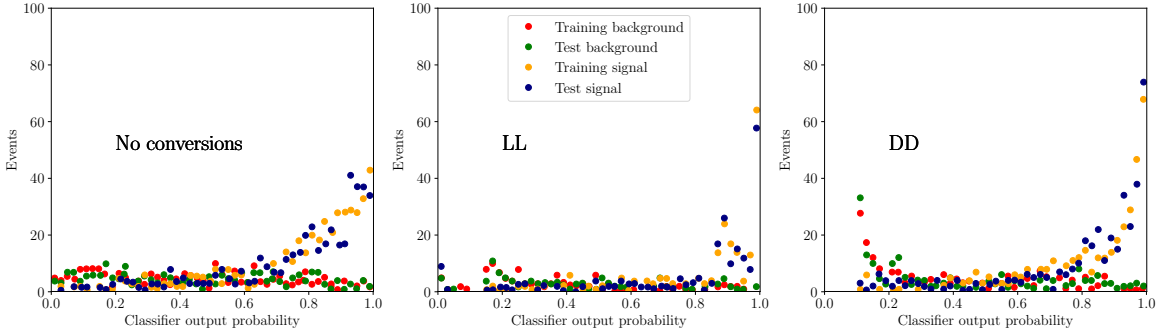


Figure 1: Training and test signal and background output distributions of the $0CV$ NN, $1CV$ DD NN, $1CV$ LL NN.

In future selection updates, k-folding [26] among other techniques can be explored to investigate if improved use of background data can be achieved.

4.3 Performance

The performance of each of the models shown in terms of ROC curves is provided in Appendix B. Ultimately, the efficiency of the models depends on the chosen working point. This is driven by resource requirements. The chosen working point of each of the models is shown in Table 4, along with the rejections and efficiencies per sample, per decay topology.

Table 4: Percentage efficiency for the B_s^0 and ALP samples relative to the reconstructed and loosely selected samples.

Efficiency (%)	<i>1CV LL</i>	<i>1CV DD</i>	<i>0CV</i>
$B_s^0 \rightarrow \gamma\gamma$	67	31	68
ALP 5 GeV	52	67	71
ALP 10 GeV	55	50	50
ALP 15 GeV	62	64	46
Rejection	85	90	85
MLP requirement	0.70	0.85	0.80

4.4 Implementation in the real-time software stack

In order to apply the neural networks in the C++ software stack used to perform event selection in real time, a conversion must take place so that the models trained in the Python implementation are reproduced.

In order to do this, the NNDRone framework [25] is used to convert the network weights and bias parameters to JSON format. This is then read in by a dedicated tool which uses the JSON parameters to initialise a LWTNN network [27] that reproduces the original model exactly. The reconstructed LWTNN model has been validated to produce identical outputs from the same input values.

5 Prospects

As explained in Sect. 1, the trigger strategy described in this paper is essential to improve the sensitivity of LHCb to $\gamma\gamma$ final states, especially after 2018. In this section, we describe briefly the prospects for the two benchmark analyses studied: the search for the rare decay $B_{(s)}^0 \rightarrow \gamma\gamma$ and that of an ALP decaying to a pair of photons. It should be noted that the same final state could also be sensitive to other models, such as that of a composite Higgs including light scalars [28].

During the full LHCb Run 2 data-taking, selections providing high efficiencies for the reconstruction of $B_{(s)}^0 \rightarrow \gamma\gamma$ decays were included (see Tab. 2 and Tab. 4). In the same regard, the efficiencies for an ALP with a mass close to that of the $B_{(s)}$ meson is also very high for that period. For the case of an ALP with a mass between $\sim 6 \text{ GeV}/c^2$ and $\sim 12 \text{ GeV}/c^2$, only data collected in 2018 with the strategy described in this document provides significant sensitivity. A similar strategy to that used in 2018 is expected to be used during Run 3 of the LHC, in which LHCb will have been upgraded [29]. Concerning the trigger, the new design [30] including the removal of the first hardware level, should provide similar or higher efficiencies.

The efficiencies reported in this document, together with the fraction of triggered data provided in Ref. [12], are used to roughly estimate the expected sensitivity in both analyses. A $\gamma\gamma$ invariant mass resolution of $\sim 25\%$ is assumed for these studies. Additional offline discrimination against the background can be achieved by using similar but more powerful classifiers than those used in HLT2. This additional discrimination is based on the use of larger training samples and variables whose reconstruction is too slow to be performed in real time. Additional background rejections of $\sim 90\%$ can then be achieved

with associated signal efficiencies of $\sim 60\%$ for all the photon reconstruction categories included in this document.

For the $B_s^0 \rightarrow \gamma\gamma$ decay an upper limit $\mathcal{B}(B_s^0 \rightarrow \gamma\gamma) \lesssim 10^{-5}$ at 90% CL could be achieved using the Run 2 LHCb dataset. This is around two times the Belle limit, currently the most stringent. Assuming similar efficiencies and backgrounds in Run 3 of the LHC, a simple projection yields $\mathcal{B}(B_s^0 \rightarrow \gamma\gamma) \lesssim 4 \times 10^{-6}$. This assumption might not hold if the ECAL performance is affected by the larger occupancy expected in Run 3. If a more optimistic background discrimination is assumed (95% background rejection for the same signal efficiency) upper limits of $\mathcal{B}(B_s^0 \rightarrow \gamma\gamma) \lesssim 6 \times 10^{-6}$ and $\mathcal{B}(B_s^0 \rightarrow \gamma\gamma) \lesssim 2 \times 10^{-6}$ could be achieved using the Run 2 and Run 3 LHCb datasets, respectively. A discovery, should the SM prediction hold, would probably need to wait until Run 4 or a potential Phase-II LHCb upgrade [31].

Concerning a search for ALPs, estimations agree with those of Ref. [7]. For the reasons explained previously, the sensitivity with the current dataset is more limited for an ALP with a mass in the $\sim 6 - 12 \text{ GeV}/c^2$ range. In the most sensitive region, decay constants below $\sim 0.3 \text{ TeV}$ could be excluded using the LHCb Run 2 dataset. Keeping the same efficiency as in 2018 for Run 3 would provide an increase to $\sim 0.4 \text{ TeV}$ for the $\sim 4 - 12 \text{ GeV}/c^2$ mass range. No other experiment is expected to contribute to the measurement in this mass range in near future.

6 Summary

Di-photon selections were first implemented in the LHCb trigger in 2015 focusing on the B_s^0 decay. In this paper, we have detailed the selection modifications required to expand the search region to allow sensitivity to undiscovered ALPs in the 2018 trigger. In order to do this and remain within resource budgets, neural network models have been introduced using the NNDrone framework to ensure fast evaluation. This is the first time such models have been used to directly select multibody candidates in real time.

Acknowledgements

We would like to thank the LHCb simulation team for their extensive support and for generating the simulated samples used in this work. We also thank the LHCb RTA team for supporting this publication and reviewing this work. We express our gratitude to our colleagues in the CERN accelerator departments for the excellent performance of the LHC. We thank the technical and administrative staff at the LHCb institutes. We acknowledge support from CERN and from the national agencies: CAPES, CNPq, FAPERJ and FINEP (Brazil); MOST and NSFC (China); CNRS/IN2P3 (France); BMBF, DFG and MPG (Germany); INFN (Italy); NWO (Netherlands); MNiSW and NCN (Poland); MEN/IFA (Romania); MSHE (Russia); MinECo (Spain); SNSF and SER (Switzerland); NASU (Ukraine); STFC (United Kingdom); DOE NP and NSF (USA). We acknowledge the computing resources that are provided by CERN, IN2P3 (France), KIT and DESY (Germany), INFN (Italy), SURF (Netherlands), PIC (Spain), GridPP (United Kingdom), RRCKI and Yandex LLC (Russia), CSCS (Switzerland), IFIN-HH (Romania), CBPF (Brazil), PL-GRID (Poland) and OSC (USA). We are indebted to the communities behind the multiple open-source software packages on which we depend.

Individual groups or members have received support from AvH Foundation (Germany); EPLANET, Marie Skłodowska-Curie Actions and ERC (European Union); ANR, Labex P2IO and OCEVU, and Région Auvergne-Rhône-Alpes (France); Key Research Program of Frontier Sciences of CAS, CAS PIFI, and the Thousand Talents Program (China); RFBR, RSF and Yandex LLC (Russia); GVA, XuntaGal and GENCAT (Spain); the Royal Society and the Leverhulme Trust (United Kingdom).

A Neural network feature distributions

The signal and background distributions for each topology are shown in Figs. 2, 3, and 4, respectively, where “signal” refers to the combination of all signal modes.

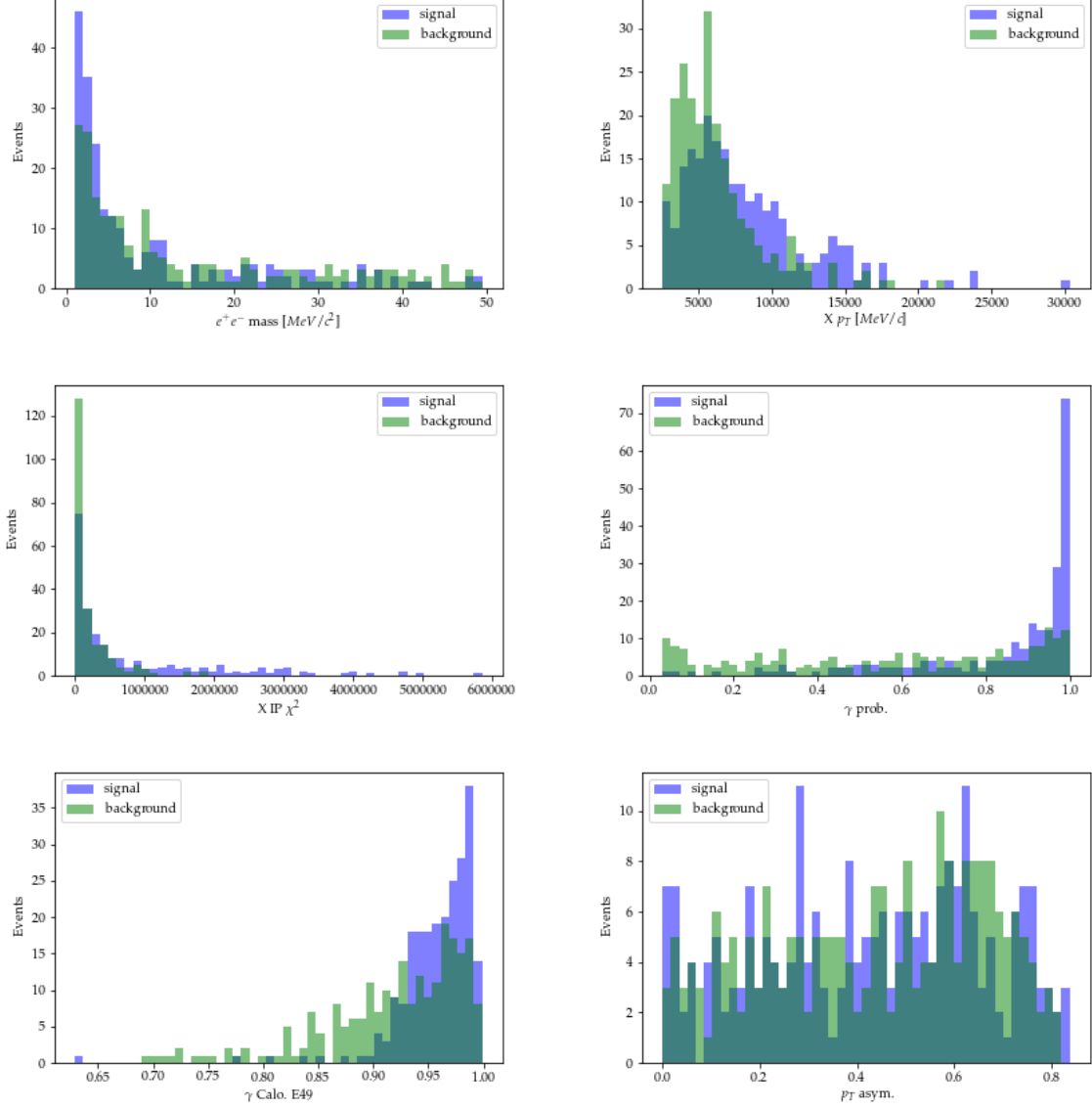


Figure 2: Signal and background distributions of information used to train the $1CV\ LL$ classifier. Variables are explained in the text.

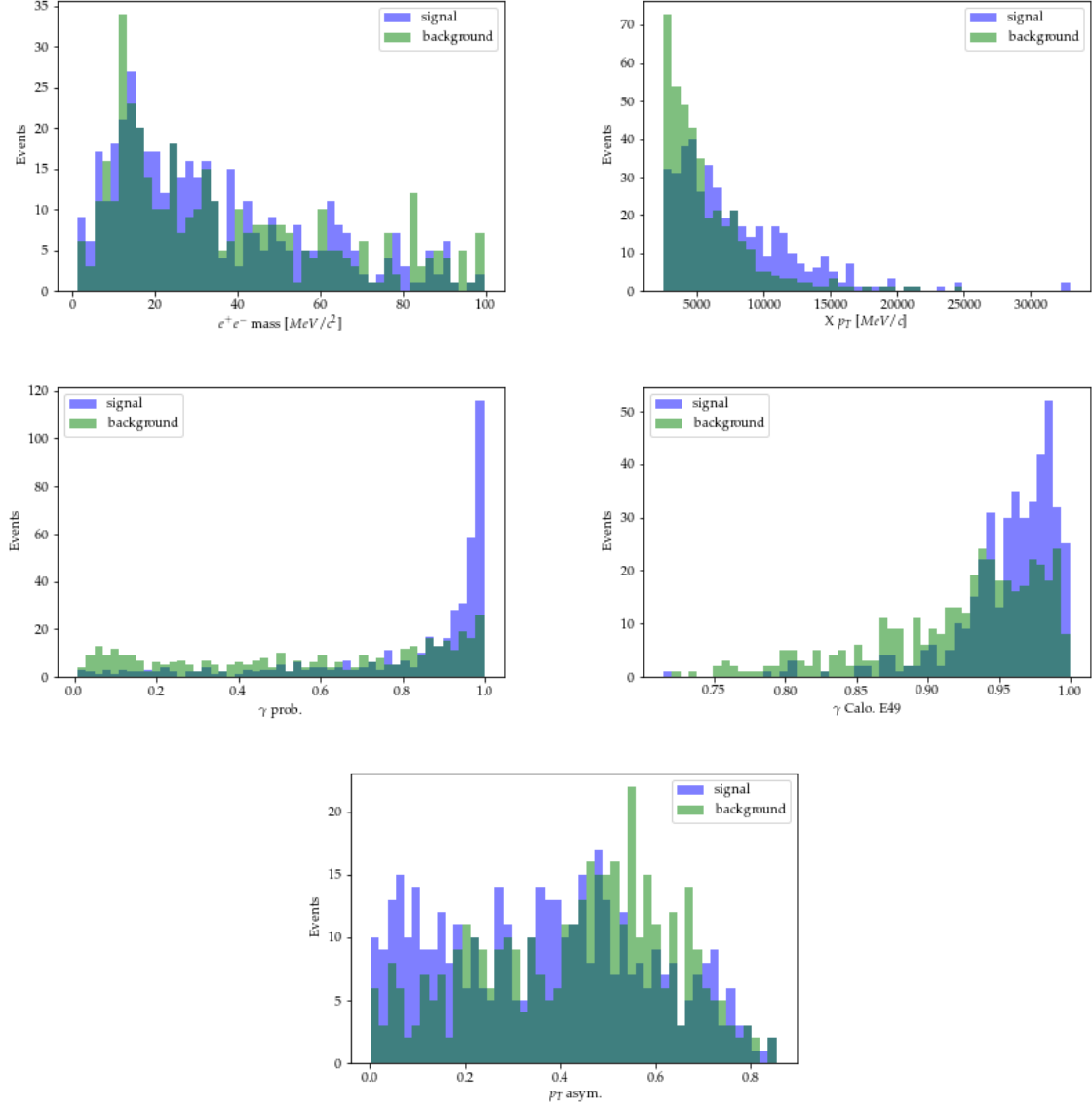


Figure 3: Signal and background distributions of information used to train the $1CV DD$ classifier. Variables are explained in the text.

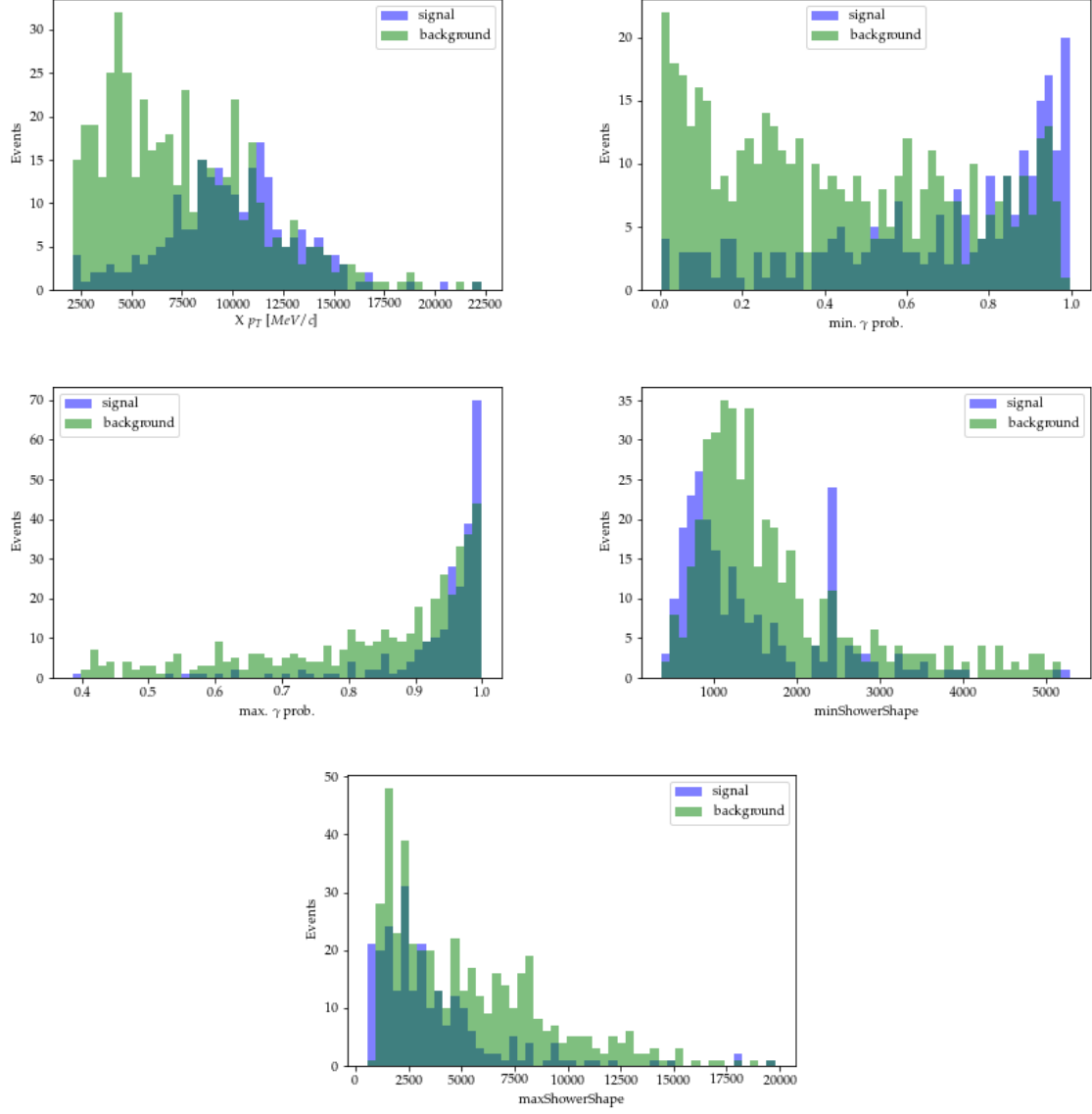


Figure 4: Signal and background distributions of information used to train the $0CV$ classifier. Variables are explained in the text.

B ROC curve performances of the NN models

The performance of each of the models is shown in terms of ROC curves in Fig. 5, which display the signal efficiency versus background rejection power.

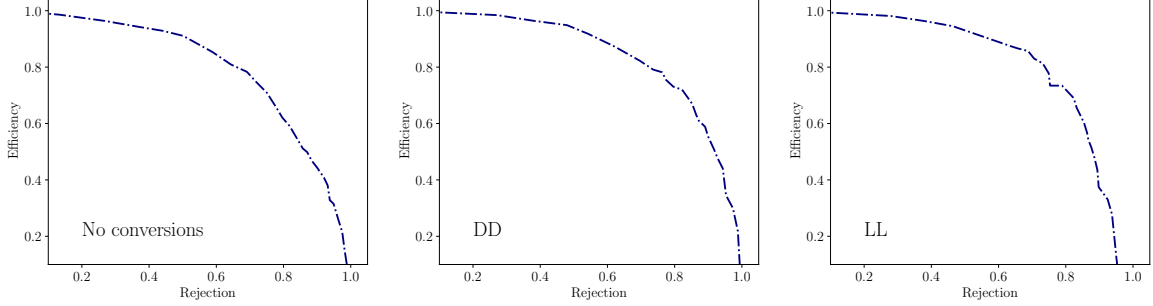


Figure 5: ROC curves for the test data using the different topologies. 0CV NN (left) , 1CV DD NN (center), 1CV LL NN (right) .

References

- [1] W.-j. Huo, C.-D. Lu, and Z.-j. Xiao, $B_{(s,d)} \rightarrow \gamma\gamma$ decay with the fourth generation, arXiv:hep-ph/0302177.
- [2] T. M. Aliev and E. O. Iltan, $B_{(s)} \rightarrow \gamma\gamma$ decay in the two Higgs doublet model with flavor changing neutral currents, Phys. Rev. **D58** (1998) 095014, arXiv:hep-ph/9803459.
- [3] A. Gemintern, S. Bar-Shalom, and G. Eilam, $B \rightarrow X_{(s)}\gamma\gamma$ and $B_{(s)} \rightarrow \gamma\gamma$ in supersymmetry with broken R -parity, Phys. Rev. **D70** (2004) 035008, arXiv:hep-ph/0404152.
- [4] Belle, D. Dutta *et al.*, Search for $B_s^0 \rightarrow \gamma\gamma$ and a measurement of the branching fraction for $B_s^0 \rightarrow \phi\gamma$, Phys. Rev. **D91** (2015) 011101, arXiv:1411.7771.
- [5] BaBar collaboration, P. del Amo Sanchez *et al.*, Search for the decay $B^0 \rightarrow \gamma\gamma$, Phys. Rev. **D83** (2011) 032006, arXiv:1010.2229.
- [6] S. W. Bosch and G. Buchalla, The double radiative decays $B \rightarrow \gamma\gamma$ in the heavy quark limit, JHEP **08** (2002) 054, arXiv:hep-ph/0208202.
- [7] X. Cid Vidal *et al.*, New Axion searches at flavor factories, JHEP **01** (2019) 113, arXiv:1810.09452.
- [8] LHCb collaboration, A. A. Alves Jr. *et al.*, The LHCb detector at the LHC, JINST **3** (2008) S08005.
- [9] D. Aloni, Y. Soreq, and M. Williams, Coupling QCD-scale axion-like particles to gluons, arXiv:1811.03474.
- [10] G. Barrand *et al.*, GAUDI - A software architecture and framework for building HEP data processing applications, Comput. Phys. Commun. **140** (2001) 45.

- [11] R. Aaij *et al.*, *Performance of the LHCb trigger and full real-time reconstruction in Run 2 of the LHC*, in preparation.
- [12] S. Benson and A. Puig Navarro, *Triggering $B_s^0 \rightarrow \gamma\gamma$ at LHCb*, Tech. Rep. LHCb-PUB-2018-006. CERN-LHCb-PUB-2018-006, CERN, Geneva, Apr, 2018.
- [13] T. Sjöstrand, S. Mrenna, and P. Skands, *PYTHIA 6.4 physics and manual*, JHEP **05** (2006) 026, arXiv:hep-ph/0603175; T. Sjöstrand, S. Mrenna, and P. Skands, *A brief introduction to PYTHIA 8.1*, Comput. Phys. Commun. **178** (2008) 852, arXiv:0710.3820.
- [14] I. Belyaev *et al.*, *Handling of the generation of primary events in Gauss, the LHCb simulation framework*, J. Phys. Conf. Ser. **331** (2011) 032047.
- [15] D. J. Lange, *The EvtGen particle decay simulation package*, Nucl. Instrum. Meth. **A462** (2001) 152.
- [16] P. Golonka and Z. Was, *PHOTOS Monte Carlo: A precision tool for QED corrections in Z and W decays*, Eur. Phys. J. **C45** (2006) 97, arXiv:hep-ph/0506026.
- [17] Geant4 collaboration, J. Allison *et al.*, *Geant4 developments and applications*, IEEE Trans. Nucl. Sci. **53** (2006) 270; Geant4 collaboration, S. Agostinelli *et al.*, *Geant4: A simulation toolkit*, Nucl. Instrum. Meth. **A506** (2003) 250.
- [18] M. Clemencic *et al.*, *The LHCb simulation application, Gauss: Design, evolution and experience*, J. Phys. Conf. Ser. **331** (2011) 032023.
- [19] J. Alwall *et al.*, *The automated computation of tree-level and next-to-leading order differential cross sections, and their matching to parton shower simulations*, JHEP **07** (2014) 079, arXiv:1405.0301.
- [20] A. Mariotti, D. Redigolo, F. Sala, and K. Tobioka, *New LHC bound on low-mass diphoton resonances*, Phys. Lett. **B783** (2018) 13, arXiv:1710.01743.
- [21] LHCb collaboration, R. Aaij *et al.*, *Measurement of the ratio of branching fractions $\mathcal{B}(B^0 \rightarrow K^{*0}\gamma)/\mathcal{B}(B_s^0 \rightarrow \phi\gamma)$ and the direct CP asymmetry in $B^0 \rightarrow K^{*0}\gamma$* , Nucl. Phys. **B867** (2013) 1, arXiv:1209.0313.
- [22] LHCb collaboration, R. Aaij *et al.*, *Observation of photon polarization in the $b \rightarrow s\gamma$ transition*, Phys. Rev. Lett. **112** (2014) 161801, arXiv:1402.6852.
- [23] LHCb collaboration, R. Aaij *et al.*, *First experimental study of photon polarization in radiative B_s^0 decays*, Phys. Rev. Lett. **118** (2017) 021801, arXiv:1609.02032.
- [24] F. Pedregosa *et al.*, *Scikit-learn: Machine learning in Python*, J. Machine Learning Res. **12** (2011) 2825, arXiv:1201.0490, and online at <http://scikit-learn.org/stable/>.
- [25] S. Benson and K. Gizdov, *NNDrone: a toolkit for the mass application of machine learning in High Energy Physics*, arXiv:1712.09114.
- [26] *Data analysis, including statistics*, Addison-Wesley, 1968.

- [27] D. H. Guest *et al.*, *lwtnn/lwtnn: Version 2.8.1*, Mar., 2019. doi: 10.5281/zenodo.2583131.
- [28] G. Cacciapaglia, G. Ferretti, T. Flacke, and H. Serodio, *Light scalars in composite Higgs models*, Front. Phys. **7** (2019) 22, arXiv:1902.06890.
- [29] LHCb collaboration, *Framework TDR for the LHCb Upgrade: Technical Design Report*, CERN-LHCC-2012-007.
- [30] LHCb collaboration, *LHCb Trigger and Online Technical Design Report*, CERN-LHCC-2014-016.
- [31] LHCb collaboration, *Physics case for an LHCb Upgrade II — Opportunities in flavour physics, and beyond, in the HL-LHC era*, arXiv:1808.08865.